RSC Advances

PAPER

View Article Online
View Journal | View Issue

Cite this: *RSC Adv.*, 2021, **11**, 24575

Ruthenium(IV) N-confused porphyrin μ-oxo-bridged dimers: acid-responsive molecular rotors†

Osamu Iwanaga,[a] Kazuki Fukuyama,[a] Shigeki Mori,[b] Jun Tae Song,[a] Tatsumi Ishihara,[a] Takaaki Miyazaki,*[a] Masatoshi Ishida*[a] and Hiroyuki Furuta*[a]

Received 30th June 2021
Accepted 5th July 2021

DOI: 10.1039/d1ra05063j

rsc.li/rsc-advances

Ruthenium(IV) N-confused porphyrin μ-oxo-bridged complexes were synthesized *via* oxidative dimerization of a ruthenium(II) N-confused porphyrin complex using 2,2,6,6-tetramethylpiperidine 1-oxyl. The deformed core planes in the dimers conferred a relatively high ring rotational barrier of *ca.* 16 kcal mol^{-1}. Rotation of the complexes was controlled by protonating the peripheral nitrogen.

The design/creation/operation of molecular rotors, gears, and switches is an interesting topic in machinery nanotechnology, allowing the development of adaptive materials, switchable chiral sensors, stereo-controlled catalysts, *etc.*[1] The molecular approach to control nanoscale motions (*e.g.*, rotation) is advantageous for realizing well-defined molecular devices or sets of practical supramolecular assembled systems.[2] As active components of molecular rotors, metal double-decker bisporphyrins and related macrocycles (*e.g.*, phthalocyanines) are representative candidates that afford specific features, such as long-term stability, ease of fabrication, and visual responses that are detectable by microscopy (Fig. 1a).[3] Bis-metal μ-oxo (or nitride)-bridged porphyrin complexes are also considered alternatives for modulating complexes' rotational mode. However, there are few investigations concerning molecular rotation because of the limitation in synthesizing molecular rotamers comprising unsymmetrical core skeletons with diamagnetic and oxophilic metal ions (for which the rotational dynamics can be probed by NMR spectroscopy) (Fig. 1b).[4]

To develop new rotors based on metal μ-oxo-bridged porphyrin dimers, we envisioned that a C_s-symmetric N-confused porphyrin (NCP) isomer possessing an inverted pyrrole ring in the macrocyclic scaffold could act as an alternative ring motif for the complexes (Fig. 1c).[5] The NCPs bind various metal ions at the NNNC core, forming unique organometallic complexes.[5,6] For example, redox-active metal species such as iron facilitate the generation of metal–oxo linkages to form μ-oxo-bridged dimer complexes.[7] In the case of iron-coordination of NCP, a unique bis-iron μ-hydroxo-bridged NCP dimer was developed, in which the structure was restricted by the coordination of peripheral sodium, as evident from X-ray crystallography (Fig. 1d).[6]

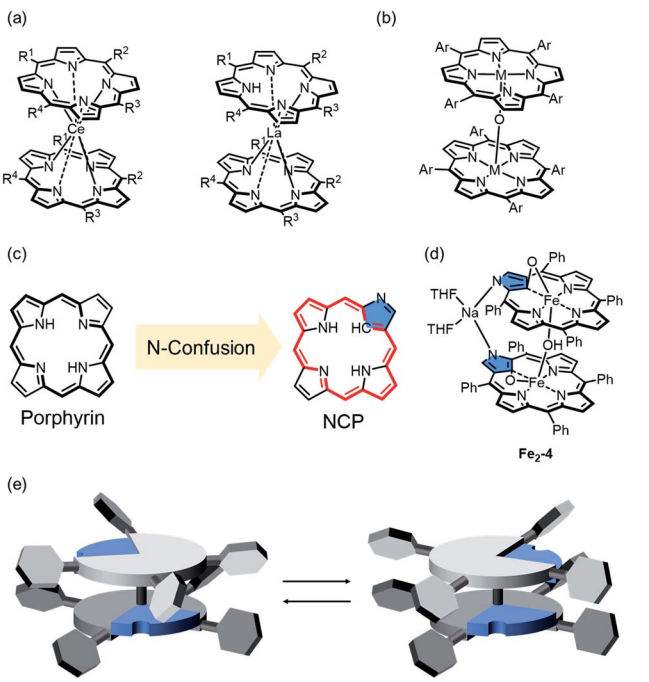

Fig. 1 Chemical structures of (a) double-decker metal porphyrin complexes and (b) bis-metal μ-oxo-bridged porphyrin complex as representative motifs of molecular rotors ($R^1 = R^3 = p$-methoxyphenyl, $R^2 = R^4 = 4$-pyridyl). (c) N-confused porphyrin as a key rotor ligand and its (d) bis-iron μ-hydroxo-bridged porphyrin complex. (e) Schematic of the rotational mode of unsymmetrical N-confused porphyrin μ-oxo dimer complex. Sky-blue moiety in the planes is a confused pyrrole ring.

[a]*Department of Applied Chemistry, Graduate School of Engineering, Center for Molecular Systems, Kyushu University, Fukuoka 819-0395, Japan. E-mail: t.miyazaki@fukuoka-u.ac.jp; ishida.masatoshi.686@m.kyushu-u.ac.jp; hfuruta@cstf.kyushu-u.ac.jp*

[b]*Advanced Research Support Center, Ehime University, Matsuyama 790-8577, Japan*

† Electronic supplementary information (ESI) available. CCDC 2076068 and 2076069. For ESI and crystallographic data in CIF or other electronic format see DOI: 10.1039/d1ra05063j

We herein report the synthesis of novel ruthenium(IV) NCP μ-oxo-bridged dimers (**Ru_2-2** and **Ru_2-3**) as a porphyrin-based molecular rotor. The ruthenium(II) NCP complex (**Ru-1**) with an axial carbonyl and pyridine (=py) exhibits catalytic reactivity for alkene epoxidation (Scheme 1).[8] The simultaneous formation of isomers can be anticipated owing to the two stereogenic centers in the NCP planes of **Ru_2-2** and **Ru_2-3**, which differ in the relative position of the nitrogen atoms of the confused pyrrole rings in the scaffold. The Ru–μ-oxo dimers showed distinct ring rotation in solution when probed *via* NMR spectroscopy (Fig. 1e). Moreover, symmetry-dependent restriction of the rotation was achieved through protonation at the peripheral imino-nitrogen moieties in **Ru_2-2** and **Ru_2-3** using trifluoroacetic acid (TFA).

Treatment of monomer **Ru-1** with 2,2,6,6-tetramethylpiperidine 1-oxyl (TEMPO) in refluxing *o*-dichlorobenzene solution under argon atmosphere afforded two products with approximately the same yields (40% each) (Scheme 1). The fast atom bombardment mass spectra of the two products revealed identical parent ion peaks at 1474.2407 (M^+) and 1474.2400 (M^+), indicating dimeric ruthenium NCP structures (*i.e.*, **Ru_2-2** and **Ru_2-3**) bridged by an oxygen atom and two axial oxygen atoms (Fig. S1 in ESI†). A characteristic broad feature tailing up to 900 nm was observed in the absorption spectra of both **Ru_2-2** and **Ru_2-3** (Fig. S2†).

The structures of **Ru_2-2** and **Ru_2-3** were unambiguously characterized by single-crystal X-ray diffraction analysis (Fig. 2 and Tables S1 and S2 in ESI†). In both complexes, two ruthenium atoms coordinated at the NNNC core in the NCPs are bridged by an oxygen atom to form a sandwich-like structure. The characteristic metalaoxirane structure was found at the inner carbons of the confused pyrrole moieties in the scaffolds.[6,9] Such oxidative reactivity is a characteristic of Ru–NCP, which is in sharp contrast to the reactivity of the Ru^{II}(CO) azuliporphyrin with an NNNC core.[10] Notably, the confused pyrrole rings in **Ru_2-2** and **Ru_2-3** are positioned opposite to the C17–Ru1–Ru2–C62(C61) torsion angle of 149.9(2)°, which is anticipated to induce molecular dipole moments. The strict structural difference between **Ru_2-2** and **Ru_2-3** is found in the position of the nitrogen atoms of the confused pyrrole rings; the former product (**Ru_2-2**) was eluted in the less polar fraction (R_f = 0.125) *via* silica gel chromatography using toluene/ethyl acetate (v/v = 19/1) and can be regarded as a *syn* conformer, whereas the polar fraction (R_f = 0.014) obtained under the same chromatographic conditions was eventually determined to be an *anti*-conformer (**Ru_2-3**).[11] The Ru1/2–O3 lengths for **Ru_2-2** and **Ru_2-3** are 1.792(3)/1.804(3) Å and 1.796(2)/1.800(2) Å, respectively, which are typical of μ-oxo-bridged ruthenium(IV) porphyrin complexes (*e.g.*, $[Ru^{IV}(TPP)(p\text{-}OC_6H_4CH_3)]_2$–O: 1.789(11) Å).[12] The bond angles of Ru1–O3–Ru2 for **Ru_2-2** and **Ru_2-3** are almost linear 175.9(2)° and 176.1(2)°, respectively, similar to those of other reported ruthenium porphyrin μ-oxo dimer complexes (*e.g.*, 177.8(7)°).[12] Due to the internal metal oxirane moieties, the confused pyrrole rings are inclined inward. Therefore, the overall geometries of the NCP planes are nonplanar with estimated mean plane deviation values (defined by 24 atoms of NCP skeleton) of 0.276 Å and 0.294 Å for **Ru_2-2** and 0.286 Å and 0.292 Å for **Ru_2-3**.

As anticipated above, the formal oxidation state of both ruthenium centers is expected to be +4 (d^4) for the complexes. The X-ray photoelectron spectra of **Ru_2-2** and **Ru_2-3** revealed higher Ru ($3p_{3/2}$) binding energies of 462.2 and 462.1 eV, respectively, than that of the divalent ruthenium (d^6) complex, **Ru-1** (460.9 eV, Fig. S3 in ESI†).

The structures of **Ru_2-2** and **Ru_2-3** were further characterized by ^{1}H NMR spectroscopy in 1,1,2,2-tetrachloroethane-d_2 (TCE-d_2) (Fig. 3a and b). At 298 K, complicatedly overlapped signals were observed in the aromatic region (7–10 ppm). To distinguish the signals from the individual groups (β-pyrrole and *meso*-phenyl) in the complexes, we prepared the deuterated-phenyl derivatives (*i.e.*, **Ru_2-2D** and **Ru_2-3D**) as shown in Scheme 1 (see, ESI†). The ^{1}H NMR spectra of **Ru_2-2D** and **Ru_2-3D** (Fig. S4†) show two singlets at 9.38 and 8.98 ppm for **Ru_2-2** and 9.32 and 9.05 for **Ru_2-3**. The remaining six β-CHs are expected to have signals around 8 ppm for both complexes. This spectral feature suggests the existence of two possible rotational isomers in solution with an almost 1 : 1 molecular ratio. The 1D exchange nuclear Overhauser effect spectra revealed chemical exchange of the rotamers at 298 K (Fig. S5 and S6†), which

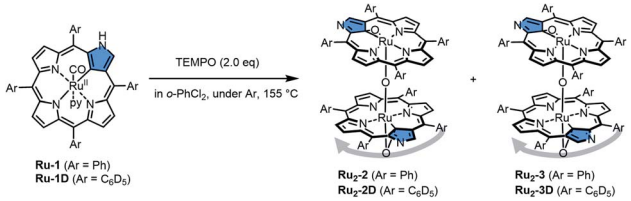

Scheme 1 Synthesis of ruthenium(IV) NCP μ-oxo dimers, **Ru_2-2** and **Ru_2-3**.

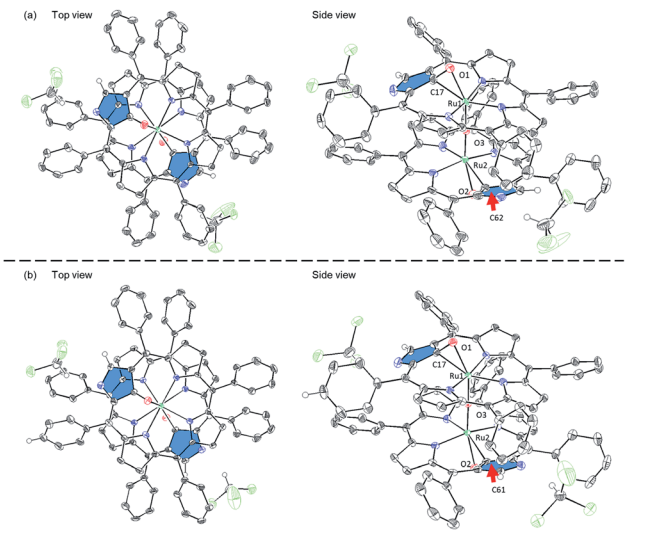

Fig. 2 Top (left) and side (right) views of crystal structures of (a) **Ru_2-2** and (b) **Ru_2-3** with thermal ellipsoids set at 50% probability level. Hydrogen atoms and solvent molecules excepting the H-atoms hydrogen-bonded to the peripheral nitrogen atoms were omitted for clarity.

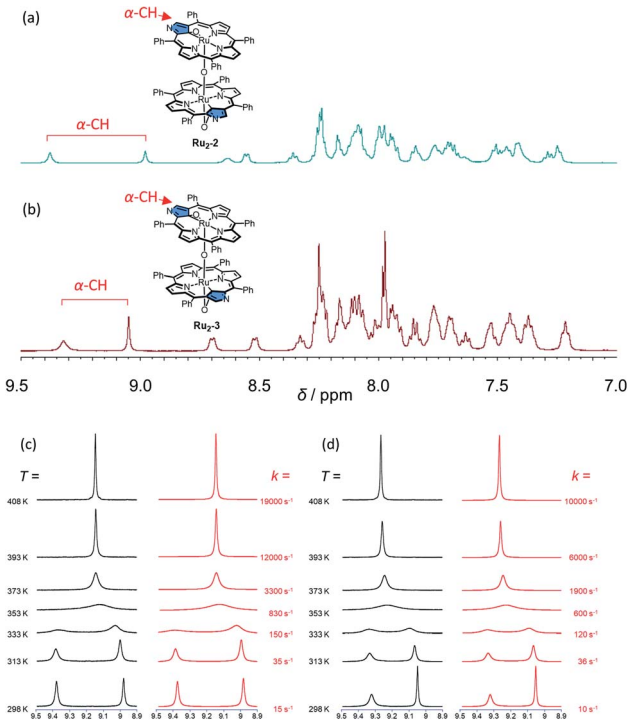

Fig. 3 ^{1}H NMR spectra of (a) Ru_2-2 and (b) Ru_2-3 recorded in TCE-d_2 at 298 K. Partial ^{1}H NMR spectra (495 MHz, black line) of (c) Ru_2-2 and (d) Ru_2-3 in TCE-d_2 as a function of temperature and the line-shape simulated spectra for the compounds (red line).

indicated that the NCP rings of **Ru_2-2** and **Ru_2-3** rotate slowly at 298 K. The rotational mode of the NCP rings was seemingly restricted at 243 K (Fig. S7 and S8†). With increasing temperature, the signal of the set of α-pyrrole protons gradually disappeared and coalesced into a single peak at 9.15 ppm for **Ru_2-2** and 9.27 ppm for **Ru_2-3** at 408 K (Fig. 3c and d). Signals of the *meso*-phenyl protons also appeared with an averaged spectral feature in the region of 7.5–8.0 ppm (Fig. S9 and S10†). These results suggest that the rotation rate of the NCP rings is faster than the NMR timescale above 353 K. Furthermore, for the ruthenium(IV) tetrakis(phenyl)-substituted porphyrin μ-oxo dimer (*e.g.*, **Ru(TPP)$_2$O**) used as the reference complex, the inward and outward CH signals (*i.e.*, *o*- and *m*-CHs) of the *meso*-phenyl rings did not coalesce even at 408 K in the variable temperature (VT) NMR spectra (Fig. S11†). In this regard, the rotation of the bulky phenyl ring could be restricted by the spatially locked dimeric structure. The rotation mode of the NCP planes could be thus mutually un-synchronized with the rotational motion of the individual *meso*-phenyl rings.

To gain further insight into the rotational barrier of the complexes, a line-shape analysis of the VT ^{1}H NMR spectra was conducted to estimate the rate constant for interconversion (k) in the specific temperature range. The free Gibbs's energy ($\Delta G^{\ddagger} = \Delta H^{\ddagger} - T\Delta S^{\ddagger}$) of **$Ru_2$-2** and **$Ru_2$-3** was determined to be (16.0 ± 0.8) kcal mol^{-1} and (16.1 ± 0.4) kcal mol^{-1}, respectively, at 298 K, from the Eyring plots (Fig. S12†). The rate constant (k < 200 s^{-1}) at 333 K indicates that the energy barrier of the ring rotations of **Ru_2-2** and **Ru_2-3** is more significant than that of the double-decker metal complexes (k = 760 s^{-1} at 333 K).[3d] Considering the structure of the complexes, the bent confused pyrrole moieties in the planes may play an essential role in the rotational motion beyond the barrier.

Upon lowering the temperature, the ratio of the integrated α-CH signals for the rotamer mixture of **Ru_2-2** changed to 0.85 (at 9.33 ppm) and 0.15 (at 8.93 ppm) (Fig. S13†). The ratio of the two-rotamers of **Ru_2-3** also changed when the temperature was further lowered (~223 K), affording a thermodynamically stable conformer (Fig. S14†). To understand the structure-dependent features of **Ru_2-2** and **Ru_2-3**, we analyzed the thermodynamic energy profiles of the possible rotational isomers (*e.g.*, **Ru_2-2a–f** and **Ru_2-3a–c**) by theoretical calculation with the B3LYP method (Tables S3 and S4†). The most stable isomers (*i.e.*, **Ru_2-2c** and **Ru_2-3c**) obtained in the optimization process are highly consistent with the crystal structures. Notably, the torsion angles of C17–Ru1–Ru2–C61(C62) in the structures of **Ru_2-2e** and **Ru_2-3b** are −102.8° and 98.5°, respectively, indicating stability (ΔE = +1.19 and +1.45 kcal mol^{-1}, respectively) relative to **Ru_2-2c/-3c**. Therefore, two energetically close conformers are present in the solution under the experimental conditions.

The effect of protonation on the rotation of the rotamers was evaluated.[13] Upon addition of trifluoroacetic acid (TFA), the absorption spectra of **Ru_2-2** and **Ru_2-3** gradually changed with isosbestic points (Fig. S15 and S16†), reflecting protonation at the peripheral imino-nitrogen of the confused pyrrole moieties (Fig. 4a and b).[14] In both complexes, a relatively large amount of TFA (at least 8 equiv) was necessary until spectral saturation (Fig. S15a and S16a). Strikingly, in the case of **Ru_2-3**, the relatively crowded imino-nitrogen site surrounded by *meso*-phenyl rings interfered with double protonation, as seen in the acid-spectral titration change after the addition of 8 equiv. of TFA (Fig. 4d, e, S15b and S16b†). In the ^{1}H NMR spectrum, the resulting dication species of **Ru_2-2** (*i.e.*, **Ru_2-2H$_2^{2+}$**) was well-resolved, demonstrating the interlocked single isomer at 298 K, as evident from the NMR spectral features (Fig. S17a†). The

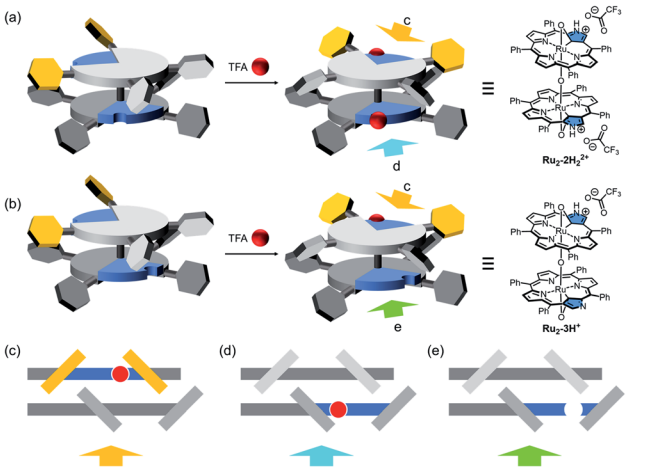

Fig. 4 Symmetry-dependent acid-binding behaviors of Ru_2-2 and Ru_2-3. Schematic of acid-induced rotational control for (a) Ru_2-2 and (b) Ru_2-3. (c)–(e) Side-views of the protonation site.

VT NMR spectra revealed that ring rotation becomes feasible with increasing temperature due to the dissociation of the TFA molecule from the complex at equilibrium (Fig. S18†). In sharp contrast, the ^{1}H NMR spectrum of the protonated species of the anti-symmetrical complex (*i.e.*, **Ru$_2$-3H$^+$**) exhibited a significantly broadened spectral feature at 298 K in TCE-d_2. The unsymmetrical spectral feature was observed at 243 K (Fig. S17b†), which may be due to the above steric issue in the conformation of **Ru$_2$-3**. Therefore, the predominant formation of mono-protonated species was anticipated in **Ru$_2$-3**. Eventually, upon the addition of triethylamine as a base, the original spectral signal of the neutral species was reproduced for both complexes (Fig. S15c and S16c†).

In summary, novel cofacial ruthenium(IV) NCP μ-oxo dimers, **Ru$_2$-2** and **Ru$_2$-3**, were synthesized as motifs for molecular rotors. The resulting complexes, **Ru$_2$-2** and **Ru$_2$-3**, are *syn*/*anti*-stereo-isomers having the nitrogen at different positions of the confused pyrrole rings. The symmetrical difference between the complexes leads to distinct rotational behavior of the Ru–NCP planes through the oxo-axis of the complex, as proven by VT ^{1}H NMR analysis. Additionally, considering the intrinsic basicity of the peripheral nitrogen sites, the rotational profile can be controlled by protonation. Further study on the cofacial metal–μ-oxo NCP dimers can enable applications in molecular machinery.

Conflicts of interest

There are no conflicts to declare.

Acknowledgements

This work was supported by Grants-in-Aid (JP19K05439, JP19H04586, and JP20H00406) from the Japan Society for the Promotion of Science (JSPS) and the Konica Minolta Science and Technology Foundation. We acknowledge support from the Cooperative Research Program of the "Network Joint Research Centre for Materials and Devices." We also acknowledge Prof. M. Watanabe for his kind advice on structural characterization.

Notes and references

1 Review see, (*a*) S. Corra, M. Curcio, M. Baroncini, S. Silvi and A. Credi, *Adv. Mater.*, 2020, **32**, 1906064; (*b*) Y.-S. Fu, J. Schwöbel, S.-W. Hla, A. Dilullo, G. Hoffmann, S. Klyatskaya, M. Ruben and R. Wiesendanger, *Nano Lett.*, 2012, **12**, 3931–3935; (*c*) J. Wang and B. L. Feringa, *Science*, 2011, **331**, 1429–1432; (*d*) D. Zhao, T. M. Neubauer and B. L. Feringa, *Nat. Commun.*, 2015, **6**, 6652.

2 (*a*) T. Kudernac, N. Ruangsupapichat, M. Parschau, B. Maciá, N. Katsonis, S. R. Harutyunyan, K.-H. Ernst and B. L. Feringa, *Nature*, 2011, **479**, 208–211; (*b*) R. A. van Delden, M. K. J. ter Wiel, M. M. Pollard, J. Vicario, N. Koumura and B. L. Feringa, *Nature*, 2005, **437**, 1337–1340; (*c*) Y. Zhang, H. Kersell, R. Stefak, J. Echeverria, V. Iancu, U. G. E. Perera, Y. Li, A. Deshpande, K.-F. Braun, C. Joachim, G. Rapenne and S.-W. Hla, *Nat. Nanotechnol.*, 2016, **11**, 706–712; (*d*) S. Erbas-Cakmak, D. A. Leigh, C. T. McTernan and A. L. Nussbaumer, *Chem. Rev.*, 2015, **115**, 10081–10206; (*e*) A. Goswami, S. Saha, P. K. Niswas and M. Schmittel, *Chem. Rev.*, 2020, **120**, 125–199; (*f*) H. Ube, R. Yamada, J. Ishida, H. Sato, M. Shiro and M. Shionoya, *J. Am. Chem. Soc.*, 2017, **139**, 16470–16473.

3 (*a*) T. Komeda, H. Isshiki, J. Liu, Y.-F. Zhang, N. Lorente, K. Katoh, B. K. Breedlove and M. Yamashita, *Nat. Commun.*, 2011, **2**, 217; (*b*) J. Otsuki, Y. Komatsu, D. Kobayashi, M. Asakawa and K. Miyake, *J. Am. Chem. Soc.*, 2010, **132**, 6870–6871; (*c*) K. Miyake, M. Fukuta, M. Asakawa, Y. Hori, T. Ikeda and T. Shimizu, *J. Am. Chem. Soc.*, 2009, **131**, 17808–17813; (*d*) M. Ikeda, M. Takeuchi, S. Shinkai, F. Tani and Y. Naruta, *Bull. Chem. Soc. Jpn.*, 2001, **74**, 739–746.

4 (*a*) K. Oniwa, S. Shimizu, Y. Shiina, T. Fukuda and N. Kobayashi, *Chem. Commun.*, 2013, **49**, 8341–8343; (*b*) D. Abdullin, N. Fleck, C. Klein, P. Brehm, S. Spicher, A. Lützen, S. Grimme and O. Schiemann, *Chem.–Eur. J.*, 2019, **25**, 2586–2596; (*c*) T. Furuyama, Y. Sugiya and N. Kobayashi, *Chem. Commun.*, 2014, **50**, 4312–4314.

5 M. Toganoh and H. Furuta, *Chem. Commun.*, 2012, **48**, 937–954.

6 C.-H. Hung, W.-C. Chen, G.-H. Lee and S.-M. Peng, *Chem. Commun.*, 2002, 1516–1517.

7 T. Guchhait, S. Sasmal, F. Shah, T. Khan and S. P. Rath, *Coord. Chem. Rev.*, 2017, **337**, 112–144.

8 (*a*) T. Miyazaki, T. Yamamoto, S. Mashita, Y. Deguchi, K. Fukuyama, M. Ishida, S. Mori and H. Furuta, *Eur. J. Inorg. Chem.*, 2018, **2018**, 203–207; (*b*) T. Miyazaki, K. Fukuyama, S. Mashita, Y. Deguchi, T. Yamamoto, M. Ishida, S. Mori and H. Furuta, *ChemPlusChem*, 2019, **84**, 603–607.

9 (*a*) T. Yamamoto, M. Toganoh and H. Furuta, *Dalton Trans.*, 2012, **41**, 9154–9157; (*b*) Z. Xiao, B. O. Patrick and D. Dolphin, *Inorg. Chem.*, 2003, **42**, 8125–8127.

10 M. J. Białek, A. Białońska and L. L. Grażyński, *Inorg. Chem.*, 2015, **54**, 6184–6194.

11 There are structural disorders (occupancies = 75% and 65% for each plane in **Ru$_2$-2**; occupancies = 75% and 56% in **Ru$_2$-3**) originating from the positions of carbon and nitrogen atoms of the confused pyrrole rings in the crystals. The $CHCl_3$ solvent molecules co-crystalized in the structure point to the external nitrogen site with possible hydrogen-bonding interaction.

12 (*a*) J. P. Collman, C. E. Barnes, P. J. Brothers, T. J. Collins, T. Ozawa, J. C. Gallucci and J. A. Ibers, *J. Am. Chem. Soc.*, 1984, **106**, 5151–5163; (*b*) E. Gallo, A. Caselli, F. Ragaini, S. Fantauzzi, N. Masciocchi, A. Sironi and S. Cenini, *Inorg. Chem.*, 2005, **44**, 2039–2049; (*c*) H. Masuda, T. Taga, K. Osaki, H. Sugimoto, M. Mori and H. Ogoshi, *Bull. Chem. Soc. Jpn.*, 1982, **55**, 3887–3890; (*d*) P. Zardi, D. Intrieri, D. M. Carminati, F. Ferretti, P. Macchi and E. Gallo, *J. Porphyrins Phthalocyanines*, 2016, **20**, 1156–1165; (*e*) J.-L. Zhang and C.-M. Che, *Chem.–Eur. J.*, 2005, **11**, 3899–3914; (*f*) H. Masuda, T. Taga, K. Osaki, H. Sugimoto,

M. Mori and H. Ogoshi, *J. Am. Chem. Soc.*, 1981, **103**, 2199–2203.

13 (*a*) Y. Wu, G. Wang, Q. Li, J. Xiang, H. Jiang and Y. Wang, *Nat. Commun.*, 2018, **9**, 1953; (*b*) B. E. Dial, P. J. Pellechia, M. D. Smith and K. D. Shimizu, *J. Am. Chem. Soc.*, 2012, **134**, 3675–3678.

14 We have obtained the preliminary crystal structure of the protonated species of **Ru_2-2** from the $CHCl_3$/hexane solution in the presence of TFA. The discrete *syn* conformer possessing the C17–Ru1–Ru2–C62 torsion angle of $-150.9(4)^\circ$ was speculated in the crystal structure. See Fig. S19 in ESI.†